The impact of Gamma radiation on the corrosion properties of carbon steel and stainless steel

Talal A. Aljohani[1]*, Abdullah M. Al-Mayouf[2], Mohammed H. Geesi[3], A. Kaiba[4], Fuad Khoshnaw[5]

*[*1]National centre for corrosion technology, King Abdulaziz City for Science and Technology P.O Box 6086 , Riyadh 11442, Saudi Arabia*
[2]Electrochemistry Research Group, Chemistry Department, College of Science, King Saud University, Riyadh 11451, Saudi Arabia.
[3]Prince Sattam Bin Abdulaziz University, College of Science and Humanity Studies, Department of Chemistry, P.O. Box 83, Alkharj 11942, Saudi Arabia
[4]Prince Sattam Bin Abdulaziz University, College of Science and Humanity Studies, Department of Physics, P.O. Box 83, Alkharj 11942, Saudi Arabia
De Montfort University, Faculty of Computing, Engineering and Media, LE1 9BH, Leicester, United Kingdom, fuad.hassankhoshnaw@dmu.ac.uk,

Abstract

The present study investigates the effect of gamma radiation with different dose rates on carbon-steel and stainless steel corrosion properties examined in a sodium-chloride electrolyte [0.6M], mainly focusing on the estimation of corrosion rate using several electrochemical techniques. The corrosion properties were studied by linear polarisation (LP), Tafel plots, and electrochemical impedance spectroscopy (EIS). Results revealed that samples exposed to high radiation doses, i.e., 150 and 250 kGy, showed better corrosion resistance. After corrosion test, Fe_3O_4 (magnetite) and Fe_2O_3 (hematite) were observed in the carbon steel samples exposed to high doses as confirmed by X-ray diffraction analysis. Scanning electron microscope (SEM) images of carbon steel showed spherical grains, the sizes and number of which varied with irradiation dose. The stainless steel exposed to lower irradiation i.e., 75 kGy , showed a clear stress corrosion cracks (SCC) while only pitting corrosion were observed in the samples exposed to high irradiation dose i.e. 150 and 250 kGy.

Key Words: Gamma radiation, Carbon steel, Stainless steel, Stress corrosion cracks, Irradiation, Linear polarization. Electrochemical Impedance spectroscopy (EIS).

1. Introduction

Corrosion is the damage of the metal by electrochemical reactions and this damage has a big impact to the economy as it is cost the countries billions of dollars yearly. For example, the cost

of the metal corrosion in the USA reached $276bn in 2001[1]. The corrosion processes causes by the oxidation and reduction reactions on the metal surface and that can either occur equally over the whole unprotected surface, such as the constant corrosion, or at isolated sites on the metal [2].

Since the stainless steel has excellent corrosion resistance [1] Therefore, it was commercial used since seven decade in many applications such as food trades, mills and railway and that delivered a good information about its atmospheric performance [3]. In addition, austenitic stainless steels alloys show superior vulnerability for intergranular stress corrosion cracking (IGSCC) than do the ferritic–martensitic composites [4],[5]. In 2004, the results of separate European programmes confirmed that the carbon steel TStE 355 can be used as a corrosion-allowance container for high-level waste (HLW) and spent fuel (SF) [2]. The performance of carbon steel in this regard depends on its corrosion rate. A simulation of this environment showed that carbon steel underwent active anaerobic corrosion, which was significantly reduced after forming a magnetite film. Another study reported that a 216-mm-thick carbon-steel container enclosed by a low-permeability solid material can achieve a lifetime of 1000 years [1]

The present study investigates the effect of gamma radiation with different dose rates on commercial carbon steel and stainless steel grade AISI304 corrosion in a sodium-chloride electrolyte [0.6M], mainly focusing on the estimation of corrosion rate using several electrochemical techniques. We assumed that gamma radiation develops the corrosion resistance of the carbon steel and AISI 304 SS samples sensitively . Moreover, The irradiation-assisted stress corrosion cracking (IASCC) can afford a considerate of the degradation as the microstructure, microchemistry, and mechanical properties of the structural material itself can be transformed by the irradiation [6],[7].

2. Experimental

2.1 Sample preparation

Commercial carbon steel and stainless steel were used in this study. Samples were cut into small square samples with an area of 2 cm2 and abraded with 600-, 800-, 1200-, and 4000-grit silicon-carbide paper. Then, the samples were cleaned with acetone in an ultrasonic bath and rinsed thoroughly with deionized water.

2.2 Radiation source

The irradiation was performed using a 60Co gamma cell 220 (Nordion, Canada). Before the radiation experiments, the gamma cell was calibrated using a ferrous-sulphate solution (Fricke dosimetry). Three radiation doses were used: 70, 150, and 250 kGy. The dose rate was 4 kGy/h. The samples were dipped in a sodium-chloride solution [0.6M] and placed in the cell. Subsequently, the irradiated samples were polished again with 600-, 800-, 1200-, and 4000-grit silicon-carbide paper, after which they were cleaned with acetone in an ultrasonic bath and rinsed thoroughly with deionized water for electrochemical testing.

2.3 Characterisation and electrochemical measurements

The surface morphology of the corroded samples was investigated using a scanning electron microscope (SEM; JSM-IT300 InTouchScope™ Scanning Electron Microscope) in combination with an X-MaxN Oxford energy-dispersive X-ray spectroscopy (EDS) analyzer. The X-ray fluorescence (XRF) and X-ray photoelectron spectroscopy (XPS) analysis were performed using an energy-dispersive X-ray fluorescence spectrometer (JSX-3100RII) and K-ALPHA^{+} surface analysis (thermos scientific). The crystallinity of the structure was explored using X-ray diffraction (JEOL JDX-8030 X-ray diffractometer system) with Cu Kα radiation operating at 40 kV and 30 mA at a scan rate of 2°/min. An SP-200 Potentiostat (Bio-Logic) and a flat corrosion cell with three electrodes were used to perform electrochemical measurement. The potential scan rate for the polarization technique was 0.166 mVs-1 to ensure a steady-state condition. A linear polarization (LP) scan was applied in a short potential window of ±25 mV. The electrochemical impedance spectroscopy (EIS) was performed at the open-circuit potential, Ecorr, by applying a sinusoidal voltage between ±10 mV within a frequency range of 10 mHz to 100 kHz. The electrochemical measurements were performed after the radiation process at 298 K.

2. Results and discussion

2.1 Characterization of microstructure

The structure and phase were examined after the corrosion test by X-ray diffraction. The diffraction patterns of the unirradiated and irradiated samples are shown in Fig. 1. The unirradiated sample only shows one peak at 44.7°. This peak is related α-Fe according to JCPDS

standard card no. 06-0696. The sample irradiated with a dose of 75 kGy shows the same peak but with a higher intensity. The intensity of the peak at 44.7° considerably increased further at higher radiation levels, i.e., 150 and 250 kGy, which is similar to the XRF analysis results in Fig. 2. In addition, two new peaks corresponding to Fe_3O_4 (magnetite) and Fe_2O_3 (hematite) appeared at $2\theta = 22°$ and $2\theta = 65°$, respectively, according to JCPDS standard cards no. 19-0629 and 79-1741. However, in accordance with JCPDS standard card no. 84-0309, the peaks at $2\theta = 22°$ and $2\theta = 65°$ are probably related to the planes (012) and (300) of Fe_2O_3 (hematite). The oxidation of carbon steel originated from the formation of Fe_3O_4 and Fe_2O_3 [8–10], and their structures have been extensively investigated elsewhere [11–13].

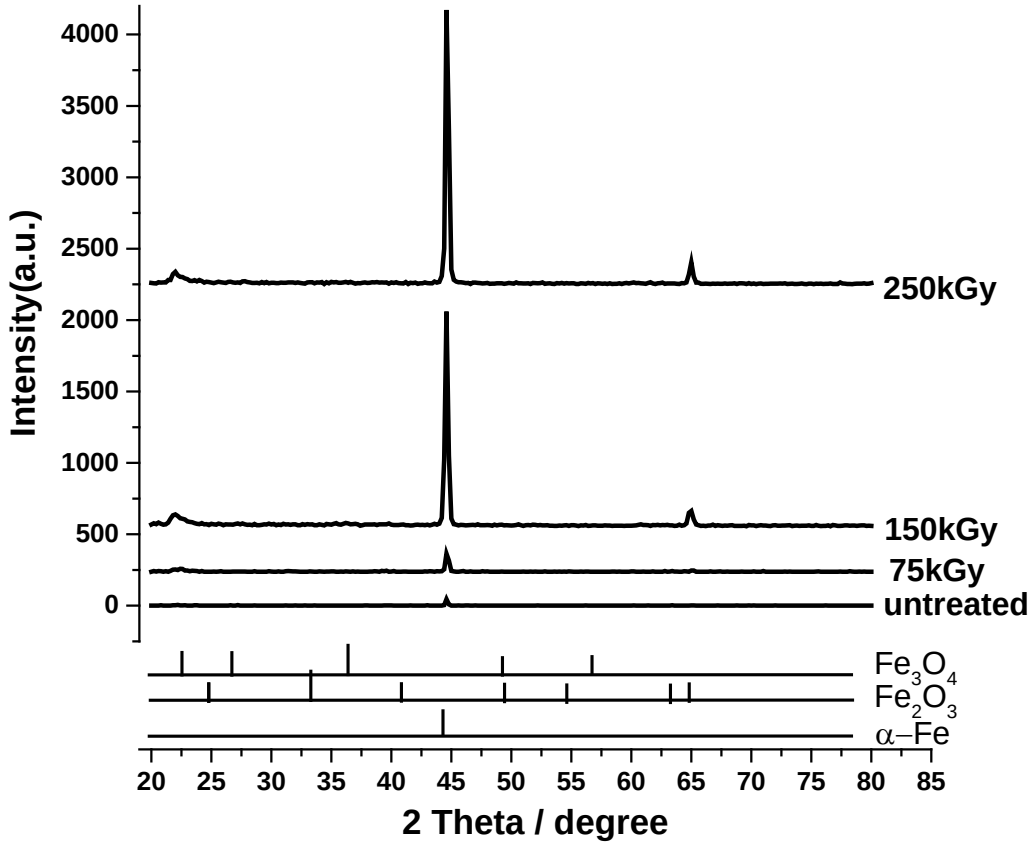

Figure 1: XRD diffraction patterns of the unirradiated and irradiated carbon-steel samples.

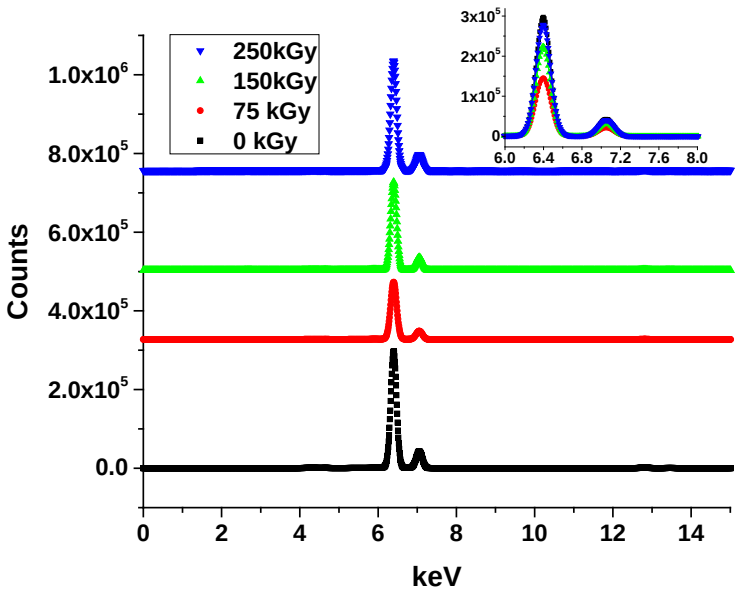

Figure 2: X-ray fluorescence analysis of the blank and irradiated carbon-steel samples. The inset shows a magnified view of the two main peaks.

For stainless steel X-ray diffraction (XRD) measurements in the range 20 (˚) – 80 (˚) with a CuKα radiation source were carried out to detect the structural changes in Stainless steel grade AISI304 irradiated with dose (75, 150 and 250 kGy) Figure 3.

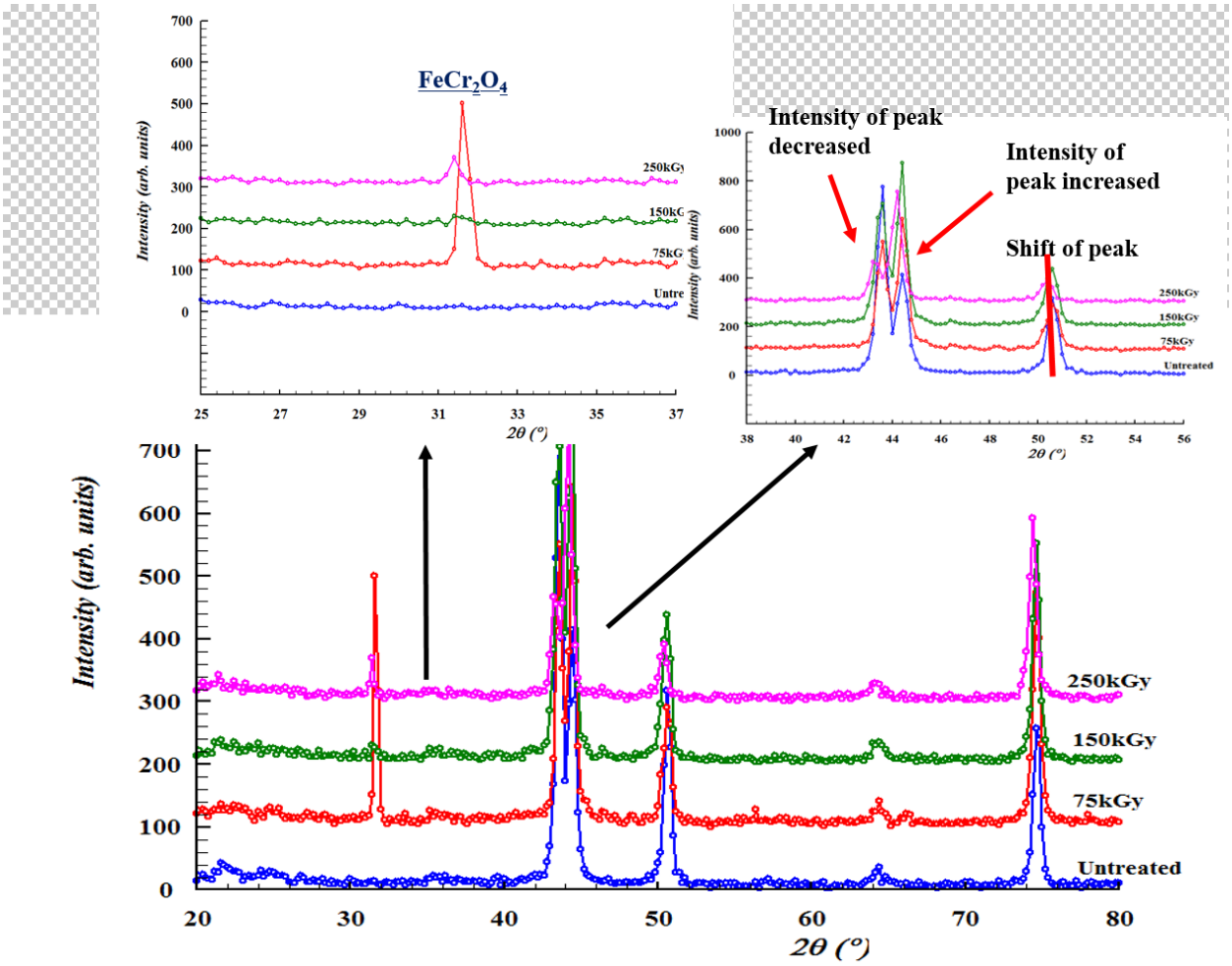

Figure 3: X-ray diffraction patterns superposition of Stainless steel grade AISI304 untreated and irradiated with dose above 75, 150 and 250 kGy.

When the sample is irradiated with a dose 75 kGy, there is presence of a new peak at (2θ=31.66˚) positions. The indexation of this pattern is shown in **Figure 3**. The program Dicvol04 [14-16], [16] and [17-18] is used to determine unit parameter cell. The best solution to index the well-defined peaks (6) gives the orthorhombic system, with a= 6.223(2) Å, b= 5.661 (2) Å,

c=3.086(1) Å and volume 108.7 $Å^3$. The Figures of merit M(6) = 54.5 and F(6) = 11.5(0.0108, 48).

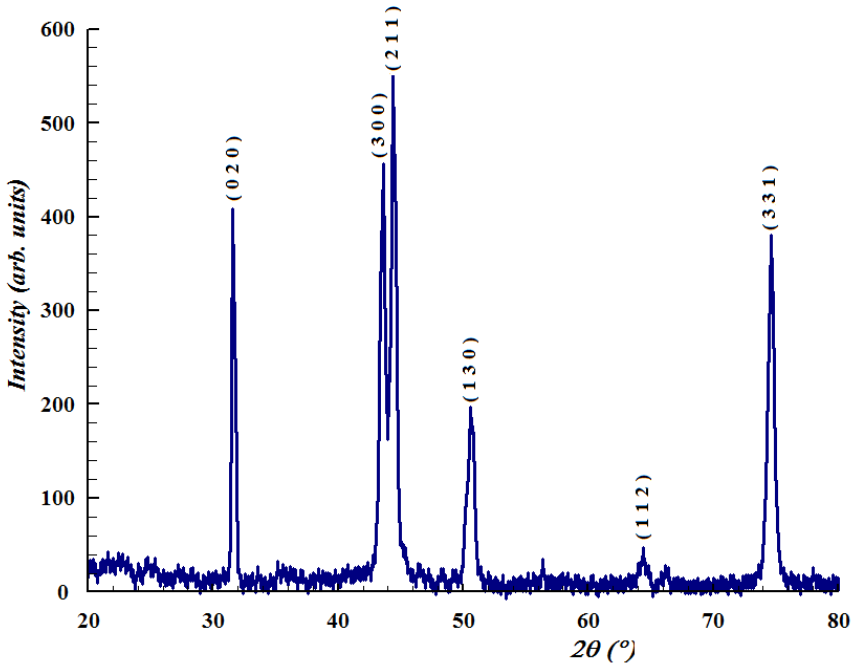

Figure.3. Indexed Diffractogram of Stainless steel grade AISI304 irradiated (75 kGy)

The intensity of this peak (020) decreases at 150kGy dose and increase after at 250 kGy. It is possible that chromium occupies the same position as iron in the octahedral sites of the crystalline structure of magnetite and that its formula can be represented as $Fe_{3-x}Cr_xO_4$ [14]. Indeed, this peak can be attributed to $FeCr_2O_4$ [15]. Also, after the phase transition the intensity of the peak at (2θ=43.60˚) positions has increased and that and that of his neighbour at (2θ=44.50˚) positions has decreased. In addition the peak at (2θ=74.65˚) undergoes a shift.

2.2 Polarisation measurements

Potentiodynamic polarisation curves for unirradiated and gamma-irradiated stainless steel AISI304 are presented in Figure 4. It is clear from the polarisation curves that gamma irradiation has increased the corrosion resistance, except for the case of 75 kGy where a reverse trend observed. The corrosion potential (E_{corr}) shifted to more negative values and the corrosion current density (I_{corr}) to more active values. For the higher irradiated samples i.e. 150 and 250, the I_{corr} reduced to more noble values with corresponding change in E_{corr}. The irradiated samples achieved the passive state at lower corrosion current densities suggesting that the gamma irradiation treatment has assisted the surface to attain the passive state quickly and more effectively.

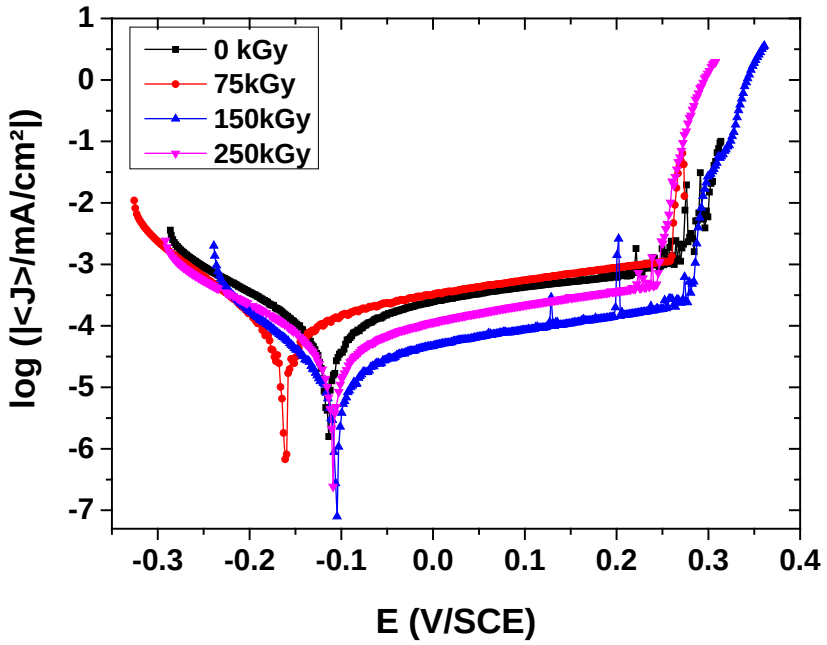

Figure 4: Potentiodynamic polarisation curves for unirradiated and gamma-irradiated stainless steel AISI304 in a sodium-chloride electrolyte [0.6M] at 298 K. The scan rate is 0.166 mV/s.

The corrosion current density for carbon steel obtained from the Tafel plots decreased gradually with increasing irradiation level, as shown in Fig. 5. Unlike the stainless steel, carbon steel show

no passivation performance. The corrosion currents for the samples treated at 150 and 250kGy display lower corrosion current densities. Although clear shift in the potential toward the negative is observed.

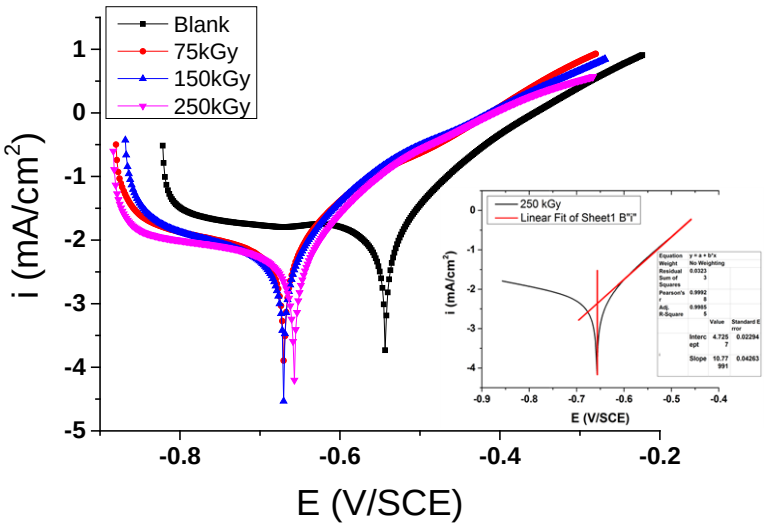

Figure 5: Potentiodynamic polarisation curves for unirradiated and gamma-irradiated carbon steel in a sodium-chloride electrolyte [0.6M] at 298 K. The scan rate is 0.166 mV/s.

Figure 6 shows the cyclic potentiodynamictests to examine the ability of the samples for achieving the passivation. The unirradiated alloy shows unstable passive layer, pits start at around 0.2V. At the reverse scan, a positive hysteresis loop is generated. The initiated pits probably will propagate. Nevertheless, the re-passivation potential E_{rep} is slightly higher than the corrosion potential E_{corr}; therefore, the surface contains merely pits as shown in Figure 7A. The stainless steel alloys exposed to 75kGy performance was entirely different. The oscillation current density at 0.3V is larger. Unlike other stainless steel samples, the re-passivation potential E_{rep} was smaller than the corrosion potential indicating that passive layer are damaged.

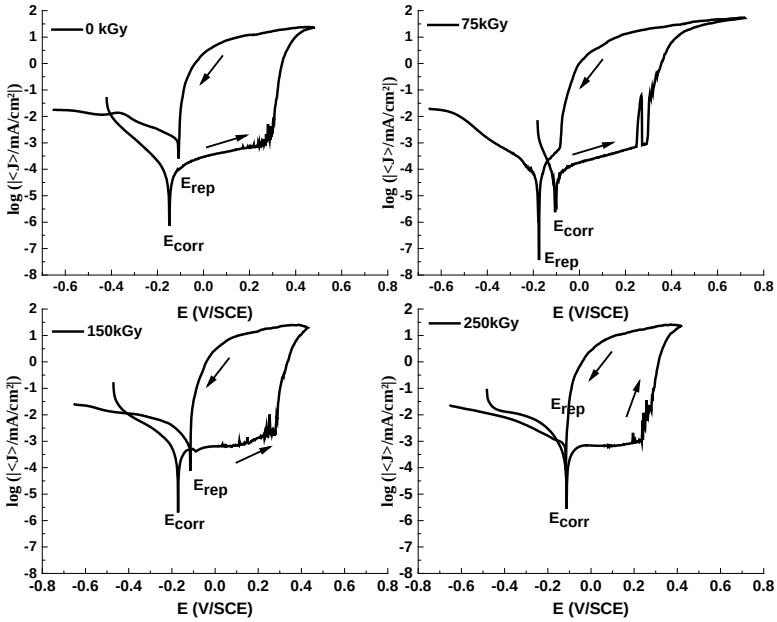

Figure 6: Cyclic potentiodynamic polarisation curves for unirradiated and gamma-irradiated stainless steel AISI304 in a sodium-chloride electrolyte [0.6M] at 298 K. The scan rate is 0.5 mV/s.

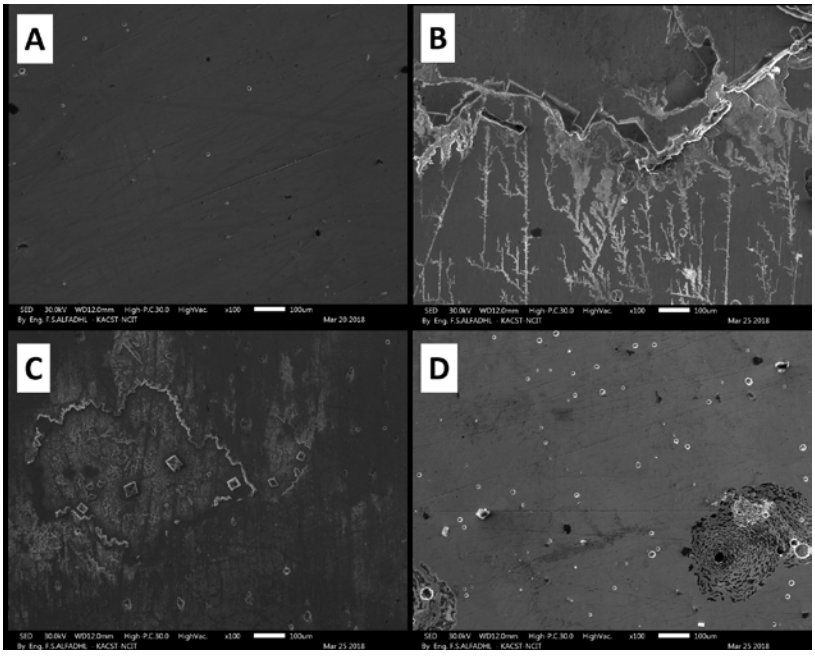

Figure 7: SEM images of stainless steel samples examined in aerated 0.6M sodium chloride at 298 K. (A) the unirradiated, (B) irradiated at 75 kGy, (C) irradiated at 150 kGy, and (D) irradiated at 250 kGy.

EIS was used to investigate the corrosion resistance performance. As shown by the Nyquist diagram in Fig. 8, the charge (corrosion) resistance initially reduced and then gradually increased with increasing irradiation dose. The semi-circular shape indicates that corrosion occurs under the charge transfer process. There is no indication of any diffusion control process at the open-circuit potential. This indicates that carbon steel has formed a protective layer of iron oxide. This layer varies with the radiation level, as shown in Fig. 8. The mechanism of how irradiation affects carbon steel corrosion resistance still uncertain. The results, however, indicate that at low irradiation level $Fe(OH)_2/Fe_3O_4$ is favourably formed by the carbon steel. At high irradiation dose, the carbon steel microstructure has changed (as displayed Fig.1) making Fe_2O_3 oxide more favourable.

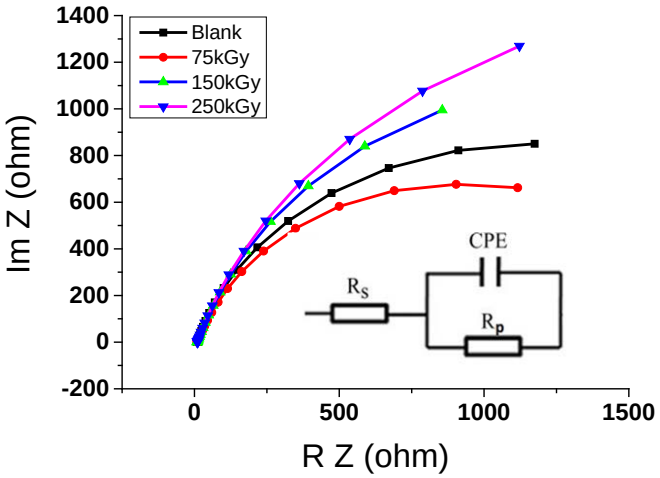

Figure 8: Nyquist plots for unirradiated and gamma-radiated carbon steel examined in a sodium-chloride electrolyte [0.6M] at 298 K. The inset figure shows the equivalent electrical circuit used to simulate EIS data.

EIS was used to investigate the corrosion resistance performance of unirradiated and gamma-irradiated stainless steel AISI304. The results are presented in Fig.9,10.

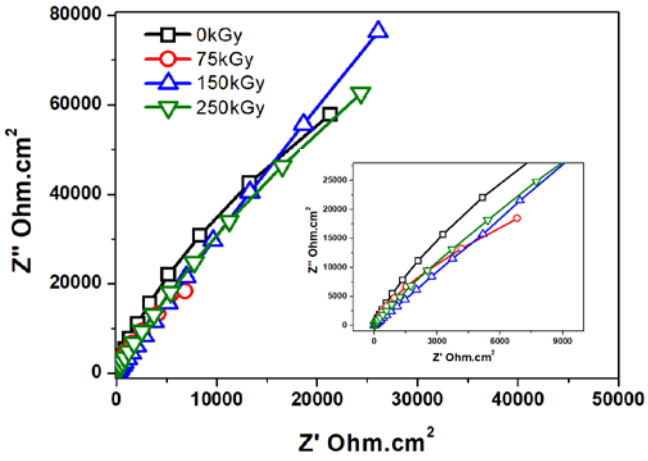

Figure 9: Nyquist plots for unirradiated and gamma-radiated stainless steel AISI304 examined in a sodium-chloride electrolyte [0.6M] at 298 K. The inset figure shows the equivalent electrical circuit used to simulate EIS data.

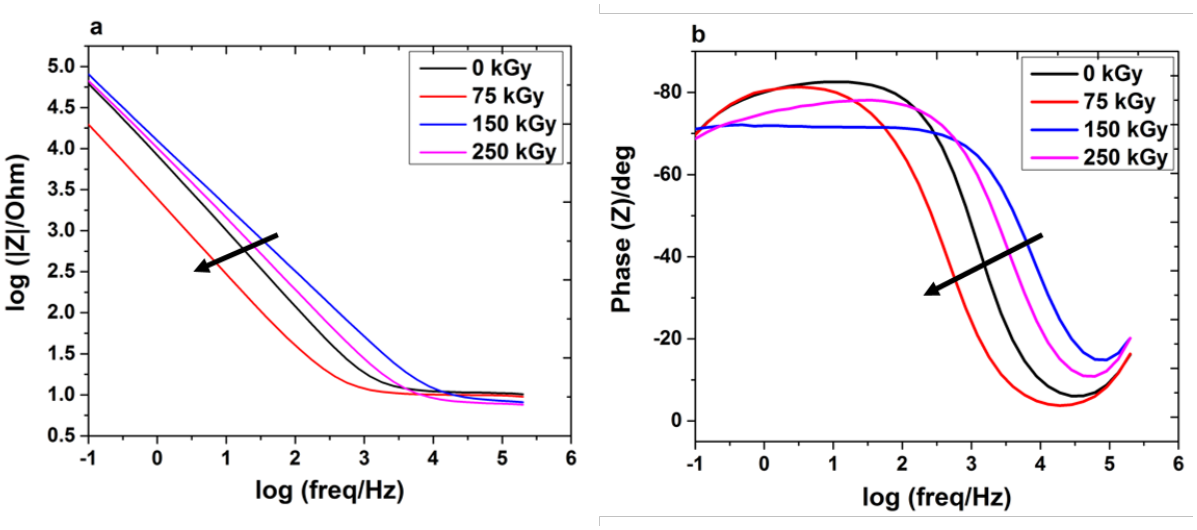

Figure 10: Electrochemical impedance diagrams (a) Bode and (b) phase angle plots for unirradiated and gamma-radiated stainless steel AISI304 examined in a sodium-chloride electrolyte [0.6M] at 298 K.

The EIS plots clearly showed the marked enhancement of the corrosion resistance of the irradiated alloy (for 150 and 250). However, similar to the polarisation plots, the 75 alloy showed a lower corrosion resistance as evident from the lower impedance values at low frequencies. Figure 9 depicts large diameter semicircle with a single time constant for all

irradiated samples. However, the time constant, to charge electrical double layer of corroding alloy, varies significantly as shown in Fig.10. The high-irradiated alloy i.e. 150 and 250 show longer (i.e. higher) time constant.

Conclusion

The effect of gamma radiation on the corrosion resistance of carbon steel was investigated in a sodium-chloride electrolyte. Three doses of gamma radiation were used. The corrosion properties were studied using the LPR method and Tafel plots. In addition, EIS was used to investigate the corrosion product layer formed on the samples. The electrochemical results revealed that the samples exposed to a high radiation dose, i.e., 150 and 250 kGy, showed enhanced corrosion resistance. Comparable results were obtained by EIS. The stainless steel exposed to lower irradiation i.e., 75 kGy , showed a clear stress corrosion cracks (SCC) while only pitting corrosion were observed in the samples exposed to high irradiation dose i.e. 150 and 250 kGy.

ACKNOWLEDGMENT

The authors are grateful to King Abdulaziz City for Science and Technology (KACST) for funding this work.

References

1. Etor, Electrochemical Measurement of Crevice Corrosion of Type AISI 304 Stainless Steel Permission to Use, 2009.
2. B. Kursten, Corrosion Evaluation of Metallic Materials for Long-Lived HLW / Spent Fuel Disposal Containers - review of 15-20 years of research, 04 (2004) 1–15.
3. S. Syed, Atmospheric corrosion of materials, Emirates J. Eng. Res. 11 (2006) 1–24. http://eclsun.uaeu.ac.ae/ejer/issues/V11/pdf_iss1_11/p1_ATMOSPHERIC_CORROSION_OF_MATERIALS.pdf.
4. G.S. Was, P. Ampornrat, G. Gupta, S. Teysseyre, E.A. West, T.R. Allen, K. Sridharan, L. Tan, Y. Chen, X. Ren, C. Pister, Corrosion and stress corrosion cracking in supercritical water, J. Nucl. Mater. 371 (2007) 176–201. doi:10.1016/j.jnucmat.2007.05.017.
5. S. Teysseyre, Z. Jiao, E. West, G.S. Was, Effect of irradiation on stress corrosion cracking in supercritical water, J. Nucl. Mater. 371 (2007) 107–117. doi:10.1016/j.jnucmat.2007.05.008.
6. H.M. Chung, W.E. Ruther, J.E. Sanecki, A. Hins, N.J. Zaluzec, T.F. Kassner, Irradiation-assisted stress corrosion cracking of austenitic stainless steels: recent progress and new approaches, J. Nucl. Mater. 239 (1996) 61–79. doi:10.1016/S0022-3115(96)00677-0.
7. M. Kodama, J. Morisawa, S. Nishimura, K. Asano, S. Shima, K. Nakata, Stress corrosion cracking and intergranular corrosion of austenitic stainless steels irradiated at 323 K, J. Nucl. Mater. 212–215 (1994) 1509–1514. doi:10.1016/0022-3115(94)91080-4.

8. A.M. Farvaque-Béra, S. Leistikow, Electrochemical studies of the corrosion behavior of a low-carbon steel in aqueous chloride solutions simulating accident conditions of radioactive waste disposal, J. Nucl. Mater. 185 (1991) 1–7.
9. Corrosion protection of low carbon steel by cation substituted magnetite (Fe3O4)., (2013).
10. S. Chang, T. Tang, K. Huang, J. Chen, Effects of Post-oxidizing Treatment on Melting Loss and Corrosion Resistance of Gas Nitrided AISI H13 Tool Steel, 52 (2012) 499–504.
11. K. Daub, X. Zhang, J.J. Noël, J.C. Wren, Gamma-radiation-induced corrosion of carbon steel in neutral and mildly basic water at 150 ° C, Corros. Sci. 53 (2011) 11–16.
12. J. Drbohlavova, R. Hrdy, V. Adam, R. Kizek, O. Schneeweiss, J. Hubalek, C. Republic, C. Republic, C. Republic, Preparation and Properties of Various Magnetic Nanoparticles, (2009) 2352–2362.
13. W. Xu, K. Daub, X. Zhang, J.J. Noel, D.W. Shoesmith, J.C. Wren, Electrochimica Acta Oxide formation and conversion on carbon steel in mildly basic solutions, 54 (2009) 5727–5738.
14. C. C. Gustavo Costa, S. Nathan Jacobson, Dorothy Lukco, W. Gary Hunter, Leah Nakley, G. Brandon Radoman-Shaw, P. Ralph Harvey, Oxidation Behavior of Stainless Steels 304 and 316 under the Venus Atmospheric Surface Conditions, Corrosion Science January, 132(2018)260-271.
15. Masafumi DOMAE, Hirotaka KAWAMURA and Taku OHIRA, Development of Alternative Reductant Application in Pressurized Water Reactor Primary Systems, Journal of Power and Energy Systems, 4(2010)62-71.
16. A Boultif, D Louër, Powder pattern indexing with the dichotomy method, J. Appl. Cryst, 37(5)(2004)724-731.
17. D Louer, M Louer, Méthode d'essais et erreurs pour l'indexation automatique des diagrammes de poudre, J. Appl. Cryst, 5(4)(1972)271-275.
18. A Boultif, D Louër, Indexing of powder diffraction patterns for low-symmetry lattices by the successive dichotomy method, J. Appl. Cryst, 24(6)(1991)987-993.